Immobilization of Uricase on Green Synthesized Gold Nanoparticles from *Ganoderma lucidum*: A Biophysical Approach to Enhanced Enzyme Stability

Firouze Mahmoudi[1], Mohammad Mirzaei[1], Masoud Torkzadeh-Mahani[2*a], Mohamad Mahani[1*b]

[1]*Department of Chemistry, Shahid Bahonar University of Kerman, Kerman, Iran.*
[2]*Department of Biotechnology, Institute of Science and High Technology and Environmental Sciences, Graduate University of Advanced Technology, Kerman, Iran.*

ABSTRACT

Gold nanoparticles (AuNPs) were synthesized using *Ganoderma lucidum* (GL) extract and applied for the immobilization of uricase enzyme derived from *Aspergillus flavus*. An eco-friendly synthesis produced spherical, stable gold nanoparticles (AuNPs) with an average diameter of 11.7 ± 6.0 nm, as confirmed by TEM, FTIR, UV–Vis spectroscopy, and EDX analyses. Uricase expressed in *Escherichia coli* BL21 (DE3) was purified using Ni–NTA Sepharose chromatography and subsequently immobilized onto the AuNPs. Spectroscopic analyses (UV-Vis and fluorescence quenching) confirmed the formation of a stable protein–AuNP complex, and quenching mechanism was studied. Thermodynamic analysis indicated that uricase binding to AuNPs is thermodynamically favorable and primarily driven by hydrogen bonding and van der Waals forces. Immobilization not only retained enzymatic activity but also enhanced the thermal stability and potential for enzyme reuse. These findings demonstrate a sustainable and efficient approach for enzyme stabilization using biogenic nanoparticles, with applications in biosensing, diagnostics, and therapeutics.

KEYWORDS

Green synthesis, Gold nanoparticles (AuNPs), Uricase immobilization, Enzyme-nanoparticle interaction, Thermodynamic analysis

Received: 9 December 2025 Revised: 21 April 2026 Accepted: 1 June 2026

INTRODUCTION

The performance of chemical and biological sensors has drastically improved by integrating with nanomaterials.[1] Au and Ag have attracted scientific attention in recent years due to their size dependent optical, electrical, chemical, and biological behaviors.[2-5] Gold nanoparticles (AuNPs) have attracted considerable research interest owing to their low resistivity and high chemical inertness.[5,6] They have demonstrated broad utility across diverse applications, including imaging,[6,7] cancer therapy,[7,8] drug delivery,[8,9] biological and chemical sensing.[9,10] Researchers are increasingly focusing on cost-effective and eco-friendly methods for AuNP synthesis, particularly green approaches that utilize biological sources such as microorganisms, algae, lichens, and plants.[11-14]

Enzymes are essential catalysts in biochemical and chemical reactions and are found universally in plants and animals.[14,15] They are valuable biocatalysts widely used in industries such as food, textile, paper, detergents, healthcare, and chemical manufacturing due to their high specificity, efficient production, and environmentally friendly nature. However, their broader application is often limited by poor long-term stability, short shelf life, and challenges in recovery and reuse. To address these limitations, enzyme immobilization has been widely proposed as an effective strategy.[15] Immobilization aims to enhance enzyme stability and reusability by anchoring the enzyme onto supports with low synthesis cost and high binding capacity. Numerous studies have explored enzyme immobilization on diverse nanoparticle platforms, including metal, metal oxide, magnetic, porous, and polymer-based nanoparticles.[16-20]

Uricase catalyzes the oxidation of uric acid to the more water-soluble product allantoin, enabling efficient renal excretion. Owing to this activity, uricase has important therapeutic and diagnostic applications, particularly in the management of hyperuricemia.[21-23] Because the enzyme is inactive in humans and higher primates, recombinant uricase (rasburicase) must be sourced from fungi, bacteria, or yeast. Among available variants, *Aspergillus flavus* uricase (Uox) is recognized as one of the most active forms and functions without requiring cofactors or metal ions.[24,25] However, recombinant Uox exhibits several limitations, including low stability, high immunogenicity, and limited solubility, which restrict its therapeutic and industrial applications. In particular, its sensitivity to elevated temperatures compromises enzyme stability and activity. Uox typically displays optimal activity within a narrow temperature range of approximately 301–303 K,[26] making temperature control an important consideration when selecting expression systems and designing production processes for recombinant enzyme production.

Recent studies have shown that immobilized uricase exhibits markedly enhanced stability, activity, and specificity compared with the free enzyme, supporting its use in the detection and degradation of uric acid in biological and food samples. A major advantage of immobilized uricase is its ability to retain catalytic activity over multiple reuse cycles, thereby reducing enzyme consumption and lowering environmental impact. Among the various immobilization platforms, metal nanoparticles—particularly gold nanoparticles (AuNPs)—have gained significant attention due to their large surface area, favorable electron-transfer properties, and excellent biocompatibility, all of which promote efficient enzyme attachment and protection against denaturation under harsh conditions.

The aim of this study is to investigate the interaction between green-synthesized gold nanoparticles (AuNPs) and uricase (Uox) to assess potential structural and functional alterations upon conjugation. The Aspergillus flavus Uox gene was expressed in *Escherichia coli* BL21 and purified using Ni-Sepharose affinity chromatography, with purity confirmed by SDS-PAGE. AuNPs were synthesized using Ganoderma lucidum extract as the reducing agent and characterized by UV–Vis and FTIR spectroscopy, TEM, and zeta potential analysis. Uox was subsequently immobilized onto the AuNP surface, and the thermodynamic parameters ΔH, ΔS, and ΔG were evaluated. This combined biophysical and thermodynamic analysis provides a basis for assessing enzyme structure and function under varying temperature conditions (The structural preservation is inferred from spectroscopic behavior, rather than directly confirmed by secondary-structure analysis).

*To whom correspondence should be addressed
Email: [a]mtmahani@gmail.com; [b]mohmahani@gmail.com

ISSN 1996-840X Online / South African Chemical Institute / http://saci.co.za/journal
© The Author(s) Published under a Creative Commons Attribution 4.0 International Licence (CC BY 4.0)
https://doi.org/10.17159/0379-4350/2026/v80se1a20

EXPERIMENTAL

Materials and equipment

Powdered Ganoderma lucidum was purchased from Iran Ganoderma. Ammonia solution (25%) was purchased from Merck (Germany), and $HAuCl_4.3H_2O$, $NaBH_4$, and ethanol (99%) were procured from Sigma-Aldrich (USA). All reagents were of analytical grade and used without further purification. IPTG and kanamycin were obtained from BioBasic Inc. (Ontario, Canada). Protein concentrations were measured using a bicinchoninic acid (BCA) assay kit (Takara, Shiga, Japan). For protein purification, a Ni–NTA Sepharose column was employed, and the pET28a (+) plasmid was sourced from Novagene (Wisconsin, USA). All remaining chemicals were obtained from Merck (Kenilworth, NJ, USA).

Fourier-transform infrared spectroscopy (FTIR, TENSOR 27) was used to characterize the Ganoderma lucidum extract and the synthesized AuNPs. UV–Vis measurements of AuNPs and protein immobilization were performed using a thermostated Cary 60 spectrophotometer (Varian, Australia). Fluorescence quenching studies were conducted with an Agilent Cary Eclipse spectrofluorometer equipped with a temperature-controlled circulating bath. The morphology and particle size distribution of the synthesized materials were evaluated by TEM. Surface charge was measured using a ZTS1240 zeta transfer standard, and elemental composition was analyzed by energy-dispersive X-ray spectroscopy (EDX).

Expression and purification of uricase

A. flavus uricase (Uox) gene sequence was synthesized by Bioneer Co. (Daejeon, South Korea) and initially inserted into the pGEM-B1 vector. Subsequently, the gene fragment was excised and ligated into the pET-28a (+) using the XhoI and NcoI restriction sites, placing it under the control of the T7 promoter. The resulting plasmid, pET-28a-Uox, underwent transfer to *Escherichia coli* BL21 (DE3) cells. Correct insertion and sequence integrity were validated by DNA sequencing.

For protein expression, the transformed *E. coli* cells were cultured and induced with 1 mM IPTG at 335 K for approximately 5 hours. After induction, the harvested cells were suspended in 50 mM Tris-HCl buffer (pH 8.5) prior to lysis by sonication on ice with 30-second pulses and 30-second rests until complete disruption. The lysate was clarified by 20 minutes' centrifugation (13,000 g, 277 K).

Purification of the His-tagged Uox was carried out at 277 K using Ni-NTA Sepharose columns (using the protocol of the manufacturer). The cell lysate containing 500 mM NaCl was applied to the column (that equilibrated with binding buffer (NaCl 500 mM, Tris-HCl 50 mM and pH = 8.0). After extensive washing to reach baseline absorbance, the bound protein underwent elution using a buffer containing 500 mM imidazole. The purity was checked via 12% SDS-PAGE, and it was subsequently concentrated with a 10 kDa cut-off Amicon centrifugal ultrafiltration device supplied (Sigma-Aldrich, Darmstadt, Germany). The concentration of the protein was quantified by a BCA assay kit.

Gold nano particles (green synthesis procedure)

Preparation of Ganoderma lucidum *extract*

A hot-water extract of *Ganoderma. Lucidum (G. lucidum)* was obtained using the reflux technique. In brief, 5.0 g of *G. lucidum* fruiting body powder was mixed with 500 mL of distilled water and heated at 358 K for 4 h under continuous stirring. The mixture was then centrifuged at 4300 rpm for 20 min to remove insoluble materials. The resulting supernatant was filtered and used for the biosynthesis of gold nanoparticles (AuNPs), while the remaining extract was stored at 277 K for further use.[14]

AuNPs synthesis

AuNPs were synthesized using a co-precipitation approach.[14] Briefly, 10 mL of a 1 mM solution of chloroauric acid was mixed with 90 mL of *Ganoderma lucidum* (*G. lucidum*) aqueous extract. The mixture's pH was adjusted to 9 using an ammonia-ammonium chloride buffer solution. The mixture was maintained at 358 K under continuous agitation (120 rpm for 6 hours). To isolate the AuNPs, the resulting suspension was treated with 95% (v/v) ethanol and centrifuged at 4000 rpm for 20 minutes. The precipitated nanoparticles were then collected and dried in an oven at 373 K for 12 hours.

Method for uricase immobilization on AuNPs

A uricase solution (0.1 mg mL^{-1}) was prepared, and 1 mL aliquots were dispensed into ten microtubes. Subsequently, 10–100 µL of a 1 mg L^{-1} gold nanoparticle (AuNP) suspension were added to each tube. The mixtures were gently agitated for 2 hours at 298 K, after which 500 µL of each sample were transferred to a fluorescence cuvette. Fluorescence emission spectra were recorded over the range of 300–450 nm at temperatures of 313, 323, and 333 K.

Uricase immobilization on AuNPs was evaluated by recording the enzyme's absorption spectra (240–300 nm) at 298 K in the presence and absence of nanoparticles using a UV–Vis spectrophotometer. Absorption titration was conducted at a fixed uricase concentration of 0.1 mg mL^{-1} while varying the AuNP concentration from 0.0 to 0.1 mg L^{-1}. In addition, shifts in the localized surface plasmon resonance (LSPR) peak of the AuNP suspension (1 mg L^{-1}) upon mixing with uricase (0.1 mg mL^{-1}) at a 1:1 ratio was analyzed to further assess protein immobilization.

Thermodynamic study

To determine the thermodynamic parameters of the interaction, fluorescence quenching of uricase was examined at varying concentrations of AuNPs. Fluorescence intensity was measured at a constant protein concentration of 0.1 mg mL^{-1} while the AuNP concentration was varied from 0.0 to 0.1 mg L^{-1}. Samples were excited at 295 nm, and emission spectra were recorded over the range of 300–450 nm at temperatures of 313, 323, and 333 K.

RESULTS AND DISCUSSION

Characterization of AuNPs

The green AuNPs were synthesized using an easy, cost-effective, and eco-friendly approach.[14] The size and shape of AuNPs were studied by TEM and as shown in Figure 1a, the nanoparticles are well-dispersed with uniform and spherical shapes. Furthermore, the corresponding histogram derived from statistical analyses, shows an average diameter of 11.7 ± 6.0 nm with a narrow distribution.

The functional groups of the GL extract and AuNPs were characterized using FTIR spectroscopy (Figure 1b). The band appearing near 3408 cm^{-1} corresponds to O–H stretching vibrations, while those at 2914 cm^{-1} and 1614 cm^{-1} arise from C–H and C=O functional groups, respectively.[14,27,28] The FTIR spectra of the gold nanoparticles show features similar to those observed in the *G. lucidum* extract, suggesting the presence of residual biomolecular functional groups on the nanoparticle surface. However, a moderate decrease in peak intensities was observed. This reduction is likely attributable to partial degradation of the *G. lucidum* extract under basic conditions (pH 9) and the oxidation of hydroxyl and carbonyl groups, processes that facilitate the reduction of Au^{3-} ions to metallic Au during nanoparticle formation.[14]

Figure 2a shows the results of zeta potential analysis. Although the measured zeta potential (~-6 mV) indicates relatively weak electrostatic stabilization, the observed colloidal stability (confirmed by electronic

absorption study during 20 days, with 5-day intervals) may be attributed to steric stabilization by biomolecules from the plant extract that act as capping agents on the nanoparticle surface. These biomolecules can create a protective organic layer that prevents nanoparticle aggregation. Furthermore, the electronic absorption spectrum of the AuNPs collide was used to analyze their optical characteristics and colloidal stability. Figure 2b shows the absorption spectra of gold nanoparticles (1.0 mg L^{-1}). The appearance of a peak at 537 nm (due to the resonance of the localised surface plasmons) confirms the synthesis of gold nanoparticles, consistent with previous studies.[14]

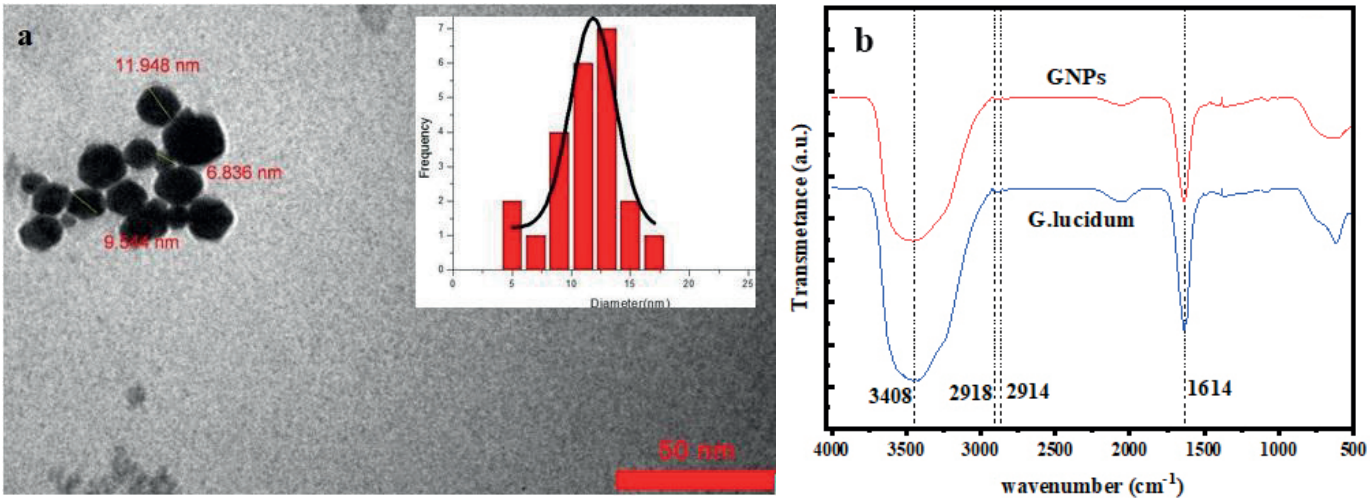


Figure 1: Size and functional group characterization of the coating on AuNPs. (a) TEM image of gold nanoparticles (AuNPs) (n~20). (b) FT-IR spectra of the Ganoderma lucidum (GL) extract and AuNPs.

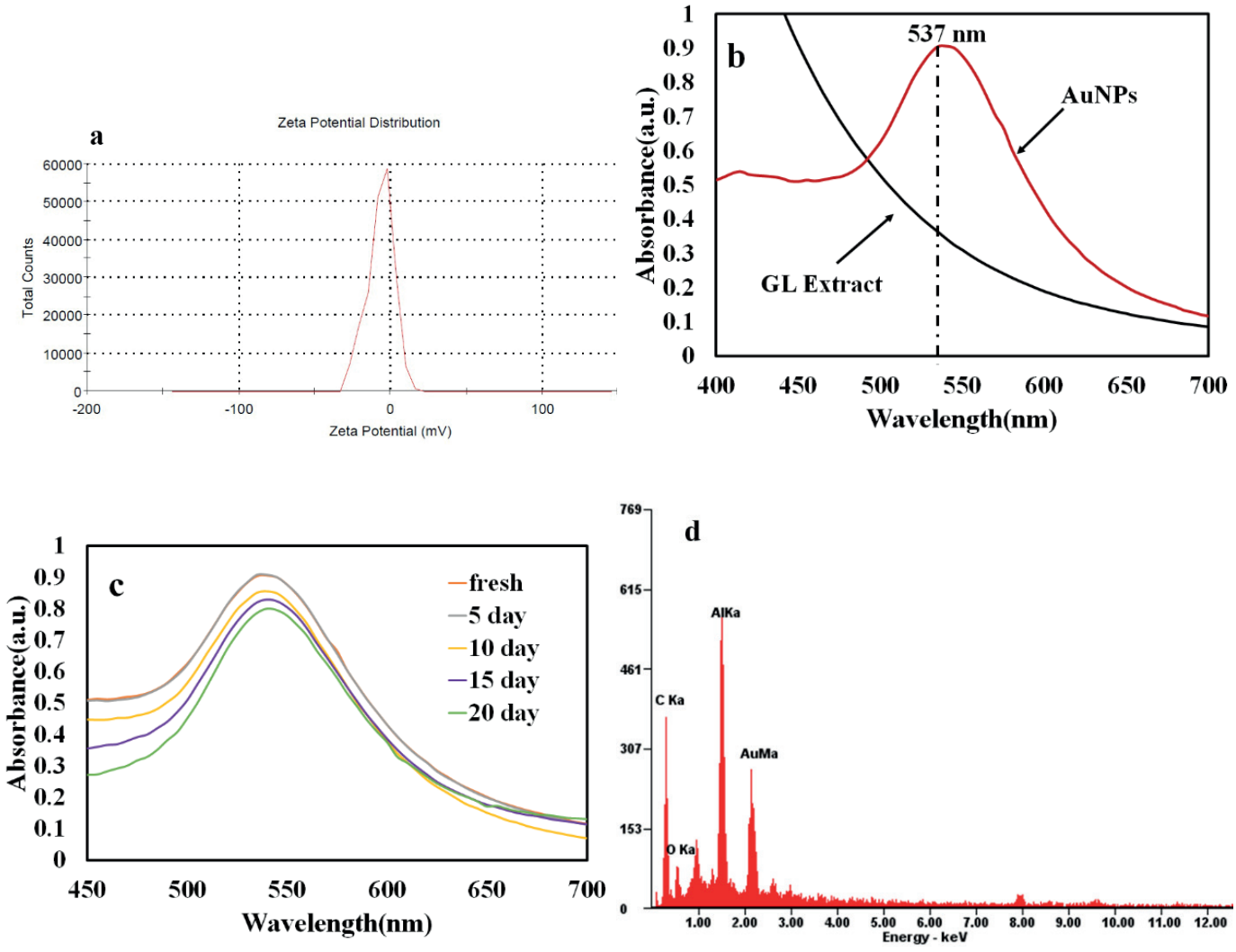


Figure 2: Physicochemical characterization of AuNPs. (a) Zeta potential of AuNPs. (b) UV–Vis absorption spectra of AuNPs (1.0 mg L^{-1}) and GL extract. (c) Stability study of AuNPs monitored by UV–Vis absorption spectroscopy over 20 days. (d) Elemental composition of synthesized AuNPs obtained by EDX.

The nanoparticle stability was also studied over 20 days, with 5-day intervals. A small change in LSPR peak at 537 nm, as shown in Figure 2c, demonstrates the nanoparticles' stability throughout this period. This stability may be attributed to a protective layer formed by *G. lucidum* extract functional groups around the AuNPs surface, effectively preventing nanoparticle agglomeration. Thus, the *G. lucidum* extract serves a dual role in AuNP synthesis as both a reducer and stabilizer.[14]

Figure 2d shows the EDX analysis for the synthesized AuNPs, where a peak at approximately 2 keV corresponds to Au Mα.[29] The main elements identified in the sample are Au, O, C, and Cl (Figure 2d). Although carbon has the highest amount at 45.64%, the amount of Au was significant at 30.35%.

Investigating the binding affinity of uricase enzyme to AuNPs

The synthesized AuNPs were coated with the uricase enzyme by mixing different concentrations of AuNPs and enzyme. Our objective was to describe the mechanisms and thermodynamic properties that control these interactions. After 2 hours of incubation at 298 K, the absorption and emission spectra of the enzyme-nanoparticle conjugates were recorded to characterize the stabilized complex and its potential application.

Study of the effect of conjugation on uricase structure

The absorption spectral assay is a widely utilized spectrometric approach that serves as a key tool for investigating structural changes in proteins, elucidating protein-nanostructure interactions, and monitoring the effects of nanostructure on enzyme.[30,31]

To investigate protein immobilization on the surface of nanoparticles using UV-Vis absorption spectroscopy, a 1:1 volume ratio of 1.0 mg L^{-1} AuNPs and 0.1 mg mL^{-1} protein solution was prepared. As shown in Figure 3, the LSPR band of the AuNPs exhibits a systematic redshift in the 500–600 nm range, which is attributed to changes in the refractive index near the particles, indicating the natural attachment of proteins. The formation of the protein corona on the AuNPs was rapid, occurring within just two minutes following their combination. Previous studies have shown a dynamic process of protein adsorption, resulting in the creation of an irreversible hard protein layer, referred to as the Protein Corona. However, this red shift cannot be directly correlated with the thickness or density of the protein layer on the nanoparticle surface, as nanoparticles of different sizes exhibit varying sensitivities to similar changes in their surrounding environment.[30]

In addition, UV-visible spectroscopy was utilized as a tool to study the impact of AuNPs on both the structural and functional properties of the uricase enzyme.[32] The UV-Vis absorption spectrum of uricase (0.1 mg mL^{-1}) was recorded in the 240–300 nm range after treatment with multiple concentrations of AuNPs (0.0–1.0 mg L^{-1}). To maintain consistent experimental conditions, a constant concentration of 0.1 mg mL^{-1} of uricase was employed across all samples to assess how nanoparticles affected the enzyme under uniform conditions. As shown in Figure S1, the gradual addition of AuNPs triggers a subtle and consistent hypochromic effect across the entire absorption spectrum, with no noticeable spectral shifts. Figure 4 illustrates the incremental reduction in absorption at the 265 nm wavelength.

Fluorescence quenching mechanism and determination of association constants

The mechanism and strength of the interaction between AuNPs and uricase (Uox) were evaluated using steady-state fluorescence methods.[33,34] As shown in Figure S2, the addition of gold nanoparticles in concentrations ranging from 0.0 to 1.0 mg L^{-1} to a uricase solution (0.1 mg mL^{-1}) has resulted in decreased fluorescence emission in the 300-450 nm wavelength (λ_{ex} = 295nm) at a temperature of 298 K. It can be concluded that the AuNPs can be bonded to uricase.

Dynamic and static quenching are among the important quenching mechanisms. Dynamic happens due to random collisions, while static quenching occurs when a complex is formed. These two mechanisms can be differentiated by changes in temperature, viscosity, or more accurately, through measuring the fluorescence lifetime.[35] Typically, as temperature increases, dynamic quenching increases because of higher diffusion rates. On the other hand, static quenching usually decreases due to the disruption of weakly bound complexes. The Stern-Volmer equation (1) is a well-known formula that explains the quenching process:

$$\frac{F_0}{F} = 1 + K_{SV}[Q] \quad (1)$$

Here, F_0 and F correspond to the fluorescence intensities measured without and with AuNPs, respectively. The quenching efficiency is quantified using the Stern–Volmer constant (Ksv), and Q represents the quencher concentration.[36,37] The Stern–Volmer constant is determined using the fluorescence quenching rate constant (k_q) and the lifetime of the protein in the absence of a quencher (τ^0), which is typically equal to 10^{-8} seconds.

The fluorescence spectra of uricase recorded at varying gold nanoparticle concentrations were analyzed to further elucidate the

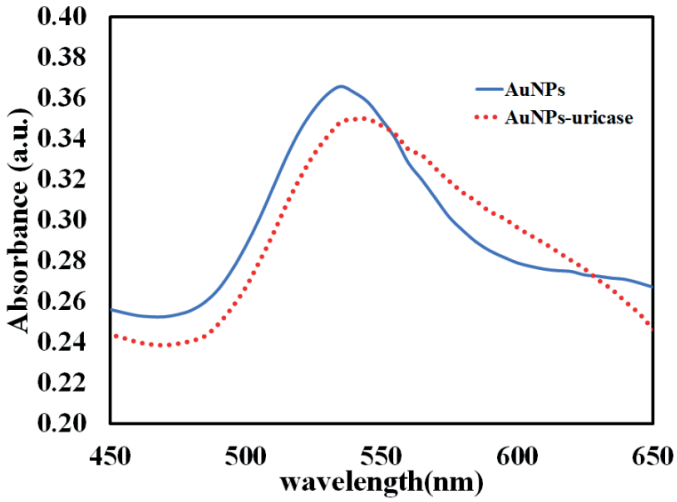


Figure 3: Confirmation of protein immobilization on the surface of AuNPs by UV–Vis absorption spectroscopy using a 1:1 volume ratio of 1.0 mg L^{-1} AuNPs and 0.1 mg mL^{-1} protein solution.

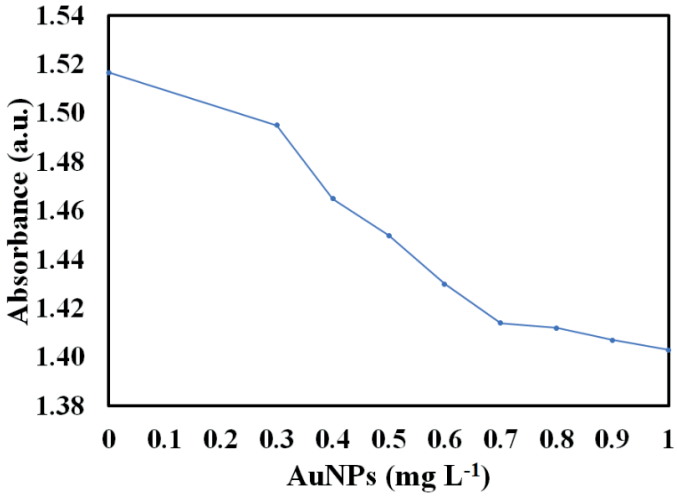


Figure 4: Plot of uricase absorbance at 265 nm as a function of AuNP concentration.

enzyme–nanoparticle interactions and to assess the influence of temperature on these binding processes. Figure 5a, 5c, and 5e show the fluorescence spectrum of uricase (0.1 mg mL^{-1}, λ_{ex} = 295nm) versus concentrations of gold nanoparticles (0.0-1.0 mg L^{-1}) and at different temperatures (313, 323, and 333 K). In all three Figures, an increase in the concentration of gold nanoparticles corresponds with a decrease in fluorescence intensity, indicating the effect of the nanoparticles on the fluorescence activity of uricase. However, at higher temperatures, this decrease in intensity occurs more gradually. Figure 5b, 5d, and 5f show the emission intensity at the maximum wavelength of 350 nm (λ_{ex} = 295 nm) versus the concentration of AuNPs (0.0-1.0 mg L^{-1}) at the same temperatures (313, 323, and 333 K). Similar to Figure 3a, 3c, and 3e, an increase in the concentration of gold nanoparticles results in a decrease in fluorescence intensity. This reduction indicates the binding of nanoparticles to uricase and its impact on the enzyme's fluorescence properties. Additionally, the more gradual decrease in intensity at higher temperatures may suggest structural changes or alterations in the environment surrounding uricase.

The ratio of the initial fluorescence intensity of uricase (F_0) at λ_{em} = 350 nm (λ_{ex} = 295 nm) to the fluorescence intensity in the presence of varying concentrations of gold nanoparticles (F), measured at the same excitation and emission wavelengths, was plotted against AuNP concentration at 313, 323, and 333 K (Figure 6).The fitting of these data results in equations in Table 1. As can be observed in equation

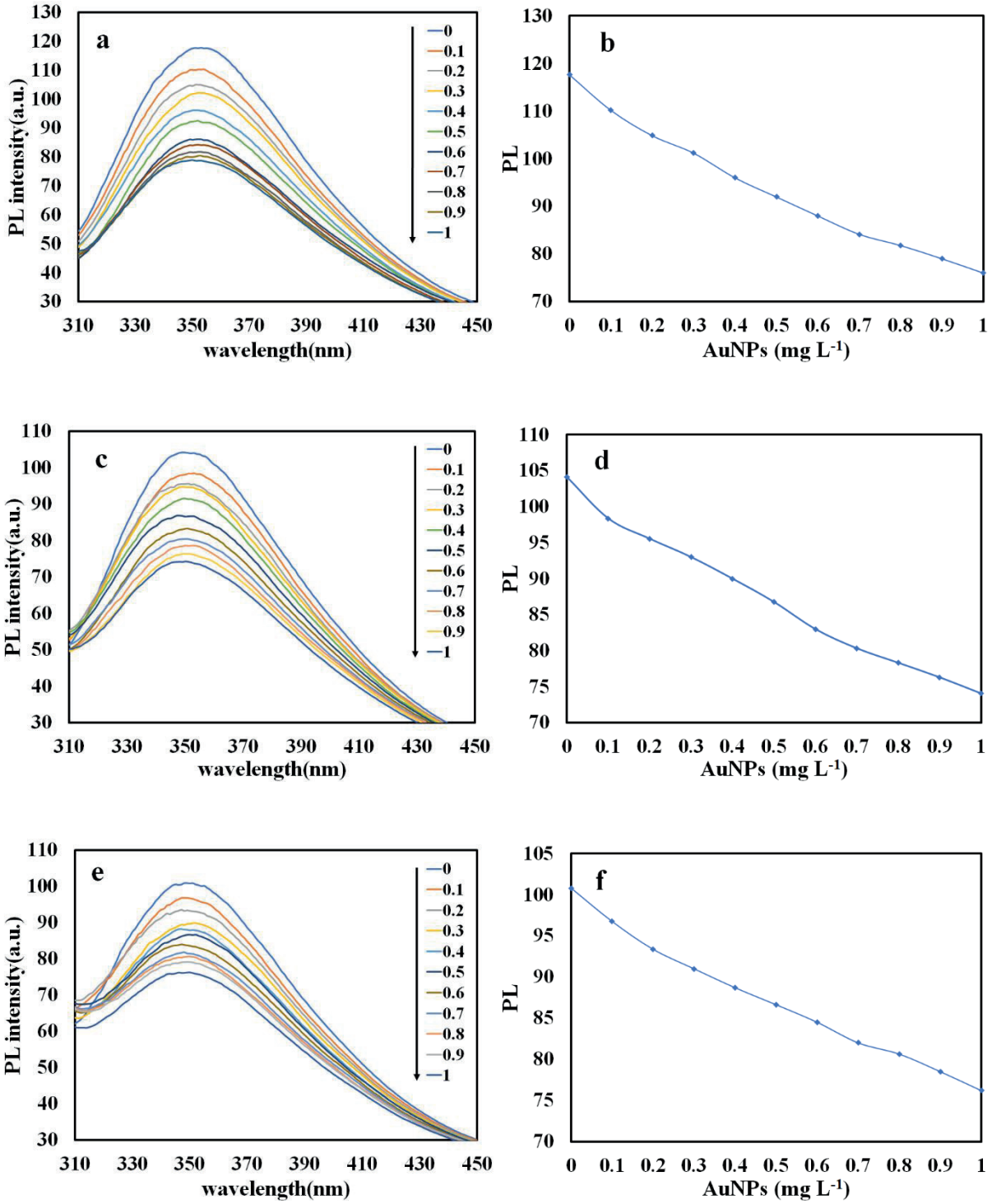


Figure 5: Fluorescence spectra of uricase (0.1 mg mL^{-1}, λ_{ex} = 295 nm) at varying AuNP concentrations (0.0 –1.0 mg L^{-1}) recorded at different temperatures: (a) 313, (c)323, and (e) 333 K. Corresponding fluorescence intensity at 350 nm plotted against AuNP concentration at (b) 313, (d) 323, and (f) 333 K.

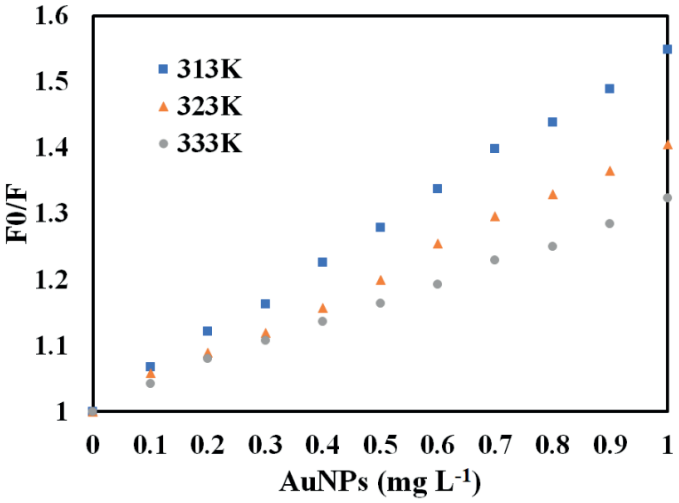


Figure 6: Stern–Volmer plot for the fluorescence quenching of uricase as a function of AuNP concentration at different temperatures.

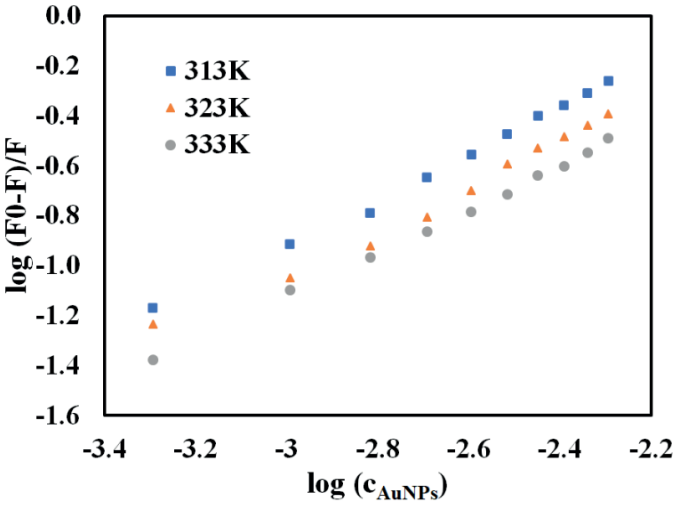


Figure 7: Log–log Stern–Volmer plot for the uricase fluorescence quenching versus AuNP concentration (in mM) at at different temperatures.

1, the slope of these equations is the Stern-Volmer constant (K_{sv}). The Stern-Volmer constant (K_{sv}) can provide significant insights into how the gold nanoparticles interact with the uricase enzyme and their effect on the fluorescence intensity. The observed decrease in the Stern–Volmer constant (K_{sv}) with increasing temperature indicates that the reduction in uricase fluorescence by gold nanoparticles (AuNPs) can be interpredted as that interaction primarily governed by a static quenching mechanism. Additionally, given that the Stern-Volmer constant is the product of the quenching constant and the protein lifetime in the absence of AuNPs ($\tau^0=10^{-8}$ s), the values of the quenching rate constant (kq) have been calculated and presented in Table 1. According to existing studies, a quenching rate constant exceeding 2×10^{10} L mol^{-1} s^{-1} illustrates a static interaction between the protein and the nanoparticle. The data recorded at each of the three temperature levels confirmed the static interaction between the gold nanoparticle and uricase.

This investigation illustrated that the interaction mechanism between AuNPs and uricase is static, leading to the formation of a stable complex. Consequently, the thermodynamic parameters that govern this interaction between the AuNPs and the protein were investigated. The binding constant (Ka) and the number of nanoparticles attached to the protein were calculated using the modified Stern-Volmer equation (2):[38]

$$\log\frac{F0-F}{F}=\log Ka+n\log[Q] \quad (2)$$

Table 1: Stern–Volmer quenching parameters of the uricase–AuNP complex measured across three temperatures.

T (K)	Equation	K_{sv} (10^3 $Lmol^{-1}$)	kq ($10^{12}M^{-1}$ S^{-1})	R^2
313	$\frac{F_0}{F}=0.054x+0.9538$	54	5.4	0.9988
323	$\frac{F_0}{F}=0.040x+0.9672$	40	4.0	0.9961
333	$\frac{F_0}{F}=0.031x+0.9793$	31	3.1	0.9972

Figure 7 shows the linear fitting of the logarithm of the fluorescence intensity ratio (LOG(F0-F)/F) plotted against the logarithm of the gold nanoparticles concentration (LOG[AuNPs]mM) for three different temperatures: 313, 323, and 333 K. Through the linear fitting performed, the values of Ka and n at the three studied temperatures were obtained and reported in Table 2.

Thermodynamic parameters of uricase and gold nanoparticle interactions

The interactions between pharmaceuticals and biological macromolecules are influenced by several non-covalent forces, including electrostatic attractions, hydrogen bonding, van der Waals interactions, and hydrophobic effects.[39,40] The magnitudes and signs of the enthalpy change (ΔH°) and entropy change (ΔS°) provide valuable insights into the dominant forces governing the binding process. To evaluate these thermodynamic parameters, Gibbs free energy (ΔG), enthalpy (ΔH), and entropy (ΔS), the Van't Hoff equation was applied to characterize the interaction between the protein and the quencher.[41]

Therefore, as shown in Figure S3, using the Van't Hoff equation (equation 3) and plotting ln (Ka) against the inverse of temperature (1/T), the changes in enthalpy and entropy can be calculated. The enthalpy is derived from the slope of the line, and the entropy from the intercept of the Van't Hoff plots. Then, the Gibbs free energy (ΔG) was calculated using equation 4. Here, R represents the universal gas constant (8.314 $J{\cdot}K^{-1}{\cdot}mol^{-1}$), T is the temperature measured in Kelvin, and K_a stands for the binding constant.

$$\ln K=-\frac{\Delta H^\circ}{RT}+\frac{\Delta S^\circ}{R} \quad (3)$$

$$\Delta G=\Delta H^\circ-T\Delta S^\circ \quad (4)$$

The thermodynamic and binding characteristics determined for the uricase–AuNPs system are shown in Table 2. The Ross et al. theory provides insights into these interactions based on thermodynamic parameters.[33,42] Values for ΔH<0 and ΔS<0 suggest predominant hydrogen bonding and van der Waals interactions and negative Gibbs free energy (ΔG<0) shows that binding interaction between gold nanoparticles (AuNPs) and uricase occurs spontaneously.

Table 2: Binding and thermodynamic characteristics of the uricase–AuNPs system measured at three temperatures.

System	T (K)	K_a ($\times10^3$ $Lmol^{-1}$)	n	Ln K_a	ΔH (kJ mol^{-1})	ΔG (kJ mol^{-1})	ΔS ($Jmol^{-1}$ K^{-1})
Uricase-AuNPs	313	69.35	0.9204	11.14	-36.06	-28.90	-22.86
	323	40.23	0.8789	10.60		-28.68	
	333	30.19	0.8674	10.31		-28.45	

CONCLUSION

In this study, immobilization of uricase onto biogenic gold nanoparticles (AuNPs) synthesized using *Ganoderma lucidum* extract significantly enhanced the enzyme's thermal stability, structural integrity, and reusability, demonstrating the effectiveness of this sustainable nanoplatform for stabilizing enzymatic activity. AuNPs synthesis using Ganoderma lucidum extract, providing a cost-effective and environmentally sustainable alternative to conventional chemical methods and the synthesized AuNPs exhibited uniform morphology, distinct optical characteristics, and strong colloidal stability. UV–Vis and fluorescence analyses confirmed the formation of stable uricase–AuNP conjugates. The negative values of ΔH and ΔS suggest that the interaction between uricase and the gold nanoparticle surface is mainly driven by hydrogen bonding and van der Waals forces, according to the thermodynamic criteria proposed by Ross and Subramanian. Collectively, these findings highlight the effectiveness of AuNPs as a robust biocompatible platform for enzyme immobilization and demonstrate the potential of plant-mediated nanoparticle synthesis for applications in biomedical and industrial biocatalysis.

SUPPLEMENTARY INFORMATION

Supplementary material is available in a separate document.

CREDIT AUTHORSHIP CONTRIBUTIONS STATEMENT

Firouze Mahmoudi: Methodology, Investigation, Formal analysis, Data curation, Writing – original draft. Mohammad Mirzaei: Conceptualization, Methodology, Validation, Resources, Supervision, Writing – review & editing. Masoud Torkzadeh-Mahani: Conceptualization, Methodology, Validation, Resources, Writing – review & editing. Mohamad Mahani: Methodology, Formal analysis, Data curation, Writing – review & editing.

DECLARATION OF COMPETING OR FINANCIAL INTERESTS

The authors declare that have no financial interests or personal relationships that could have appeared to influence the work reported in this paper.

DECLARATION OF GENERATIVE AI AND AI-ASSISTED TECHNOLOGIES

The authors declare that no generative AI or AI-assisted technologies were used in the preparation, writing, or editing of this manuscript.

AUTHORS ORCID

Firouze Mahmoudi: https://orcid.org/0009-0009-0280-5623
Mohammad Mirzaei: https://orcid.org/0000-0003-1829-1478
Masoud Torkzadeh-Mahani: https://orcid.org/0000-0002-3398-7468
Mohamad Mahani: https://orcid.org/0000-0001-5258-8561

REFERENCES

1. Leong SX, Leong YX, Koh CSL, Tan EX, Nguyen LBT, Chen JRT, Chong C, Pang DWC, Sim HYF, Liang X, et al. Emerging nanosensor platforms and machine learning strategies toward rapid, point-of-need small-molecule metabolite detection and monitoring. Chem Sci (Camb). 2022;13(37):11009–11029. https://doi.org/10.1039/D2SC02981B.
2. Fan J, Cheng Y, Sun M. Functionalized gold nanoparticles: Synthesis, properties and biomedical applications. Chem Rec. 2020;20(12):1474–1504. https://doi.org/10.1002/tcr.202000087.
3. Prosposito P, Burratti L, Venditti I. Silver nanoparticles as colorimetric sensors for water pollutants. Chemosensors (Basel). 2020;8(2):26. https://doi.org/10.3390/chemosensors8020026.
4. Grigorchuk NI. Size and shape effect on optical conductivity of metal nanoparticles. Europhys Lett. 2018;121(6):67003. https://doi.org/10.1209/0295-5075/121/67003.
5. Abdussalam-Mohammed W. Comparison of chemical and biological properties of metal nanoparticles (au, ag), with metal oxide nanoparticles (zno-nps) and their applications. Adv J Chem Sect A. 2020;3(2):192–236. https://doi.org/10.33945/SAMI/AJCA.2020.2.8.
6. Fan J, Sun M. Nanoplasmonic nanorods/nanowires from single to assembly: Syntheses, physical mechanisms and applications. Chem Rec. 2020;20(9):1043–1073. https://doi.org/10.1002/tcr.202000051.
7. Sang D, Luo X, Liu J. Biological interaction and imaging of ultrasmall gold nanoparticles. Nano-Micro Lett. 2024;16(1):44. https://doi.org/10.1007/s40820-023-01266-4.
8. Kesharwani P, Ma R, Sang L, Fatima M, Sheikh A, Abourehab MA, Gupta N, Chen Z-S, Zhou Y. Gold nanoparticles and gold nanorods in the landscape of cancer therapy. Mol Cancer. 2023;22(1):98. https://doi.org/10.1186/s12943-023-01798-8.
9. Rosyidah A, Kerdtoob S, Yudhistyra WI, Munfadlila AW. Gold nanoparticle-based drug nanocarriers as a targeted drug delivery system platform for cancer therapeutics: A systematic review. Gold Bull. 2023;56(3):121–134. https://doi.org/10.1007/s13404-023-00331-5.
10. Patil T, Gambhir R, Vibhute A, Tiwari AP. Gold nanoparticles: synthesis methods, functionalization and biological applications. J Cluster Sci. 2023;34(2):705–725. https://doi.org/10.1007/s10876-022-02287-6.
11. Santhosh PB, Genova J, Chamati H. Green synthesis of gold nanoparticles: an eco-friendly approach. Chemistry (Basel). 2022;4(2):345–369. https://doi.org/10.3390/chemistry4020026.
12. Boruah JS, Devi C, Hazarika U, Bhaskar Reddy PV, Chowdhury D, Barthakur M, Kalita P. Green synthesis of gold nanoparticles using an antiepileptic plant extract: in vitro biological and photo-catalytic activities. RSC Adv. 2021;11(45):28029–28041. https://doi.org/10.1039/D1RA02669K.
13. Vijayaram S, Razafindralambo H, Sun Y-Z, Vasantharaj S, Ghafarifarsani H, Hoseinifar SH, Raeeszadeh M. Applications of green synthesized metal nanoparticles—a review. Biol Trace Elem Res. 2024;202(1):360–386. https://doi.org/10.1007/s12011-023-03645-9.
14. Nguyen VP, Le Trung H, Nguyen TH, Hoang D, Tran TH. Advancement of microwave-assisted biosynthesis for preparing au nanoparticles using ganoderma lucidum extract and evaluation of their catalytic reduction of 4-nitrophenol. ACS Omega. 2021;6(47):32198–32207. https://doi.org/10.1021/acsomega.1c05033.
15. Ahmad R, Sardar M. Enzyme immobilization: an overview on nanoparticles as immobilization matrix. Biochem Anal Biochem. 2015;4(2):1. https://doi.org/10.4172/2161-1009.1000178.
16. Li J, Han L, Feng T, Zhang M, Jiang T. Metal-phenolic network-functionalized magnetic nanoparticles for enzyme immobilization. Appl Biochem Biotechnol. 2022;194(11):5305–5321. https://doi.org/10.1007/s12010-022-04003-6.
17. Schwaminger SP, Fehn S, Steegmüller T, Rauwolf S, Löwe H, Pflüger-Grau K, Berensmeier S. Immobilization of petase enzymes on magnetic iron oxide nanoparticles for the decomposition of microplastic pet. Nanoscale Adv. 2021;3(15):4395–4399. https://doi.org/10.1039/D1NA00243K.
18. Cheng Y, Li Z, Sun H, Zhao L, Liu Z, Cao R, Liu Q, Mao X. Immobilization of chitosanase on magnetic nanoparticles: Preparation, characterization and properties. J Ocean Univ China. 2022;21(5):1381–1388. https://doi.org/10.1007/s11802-022-5189-6.
19. Huang S, Chen G, Ouyang G. Confining enzymes in porous organic frameworks: from synthetic strategy and characterization to healthcare applications. Chem Soc Rev. 2022;51(15):6824–6863. https://doi.org/10.1039/D1CS01011E.
20. Asaduzzaman F, Salmon S. Enzyme immobilization: polymer–solvent–enzyme compatibility. Mol Syst Des Eng. 2022;7(11):1385–1414. https://doi.org/10.1039/D2ME00140C.
21. Kratzer JT, Lanaspa MA, Murphy MN, Cicerchi C, Graves CL, Tipton PA, Ortlund EA, Johnson RJ, Gaucher EA. Evolutionary history and metabolic insights of ancient mammalian uricases. Proc Natl Acad Sci USA. 2014;111(10):3763–3768. https://doi.org/10.1073/pnas.1320393111.
22. Varela-Echavarría A, de Oca-Luna RM, Barrera-Saldaña HA. Uricase protein sequences: conserved during vertebrate evolution but absent in humans. FASEB J. 1988;2(15):3092–3096. https://doi.org/10.1096/fasebj.2.15.3192041.
23. Terkeltaub R, Bushinsky DA, Becker MA. Recent developments in our understanding of the renal basis of hyperuricemia and the development

of novel antihyperuricemic therapeutics. Arthritis Res Ther. 2006;8(Suppl 1):S4. https://doi.org/10.1186/ar1909.

24. Gabison L, Chiadmi M, El Hajji M, Castro B, Colloc'h N, Prangé T. Near-atomic resolution structures of urate oxidase complexed with its substrate and analogues: the protonation state of the ligand. Acta Crystallogr D Biol Crystallogr. 2010;66(6):714–724. https://doi.org/10.1107/S090744491001142X.
25. Collings I, Watier Y, Giffard M, Dagogo S, Kahn R, Bonneté F, Wright JP, Fitch AN, Margiolaki I. Polymorphism of microcrystalline urate oxidase from aspergillus flavus. Acta Crystallogr D Biol Crystallogr. 2010;66(5):539–548. https://doi.org/10.1107/S0907444910005354.
26. Caves MS, Derham BK, Jezek J, Freedman RB. Thermal inactivation of uricase (urate oxidase): mechanism and effects of additives. Biochemistry. 2013;52(3):497–507. https://doi.org/10.1021/bi301334w.
27. Ibrahim MA, Allam M, El-Haes H, Jalbout AF, De Leon A. Analysis of the structure and vibrational spectra of glucose and fructose. Eclét Quím. 2006;31(3):15–21. https://doi.org/10.26850/1678-4618eqj.v31.3.2006.p15-21.
28. Wang J, Zhang L. Structure and chain conformation of five water-soluble derivatives of a β-d-glucan isolated from ganoderma lucidum. Carbohydr Res. 2009;344(1):105–112. https://doi.org/10.1016/j.carres.2008.09.024.
29. Fowles CC, Smoak EM, Banerjee IA. Interactions of zeatin with gold ions and biomimetic formation of gold complexes and nanoparticles. Colloids Surf B Biointerfaces. 2010;78(2):250–258. https://doi.org/10.1016/j.colsurfb.2010.03.010.
30. Piella J, Bastús NG, Puntes V. Size-dependent protein–nanoparticle interactions in citrate-stabilized gold nanoparticles: the emergence of the protein corona. Bioconjug Chem. 2017;28(1):88–97. https://doi.org/10.1021/acs.bioconjchem.6b00575.
31. Kilimci U, Uygun DA. Preparation of pegylated uricase attached magnetic nanowires and application for uric acid oxidation. J Biotechnol. 2023;373:12–19. https://doi.org/10.1016/j.jbiotec.2023.06.005.
32. Chakraborty M, Paul S, Mitra I, Bardhan M, Bose M, Saha A, Ganguly T. To reveal the nature of interactions of human hemoglobin with gold nanoparticles having two different morphologies (sphere and star-shaped) by using various spectroscopic techniques. J Photochem Photobiol B. 2018;178:355–366. https://doi.org/10.1016/j.jphotobiol.2017.11.026.
33. Yin M-M, Dong P, Chen W-Q, Xu S-P, Yang L-Y, Jiang F-L, Liu Y. Thermodynamics and mechanisms of the interactions between ultrasmall fluorescent gold nanoclusters and human serum albumin, γ-globulins, and transferrin: A spectroscopic approach. Langmuir. 2017;33(21):5108–5116. https://doi.org/10.1021/acs.langmuir.7b00196.
34. Liu J, Peng Q. Protein-gold nanoparticle interactions and their possible impact on biomedical applications. Acta Biomater. 2017;55:13–27. https://doi.org/10.1016/j.actbio.2017.03.055.
35. Feng G, Zhang H, Zhu X, Zhang J, Fang J. Fluorescence thermometers: intermediation of fundamental temperature and light. Biomater Sci. 2022;10(8):1855–1882. https://doi.org/10.1039/D1BM01912K.
36. Tu B, Wang Y, Mi R, Ouyang Y, Hu Y-J. Evaluation of the interaction between naringenin and human serum albumin: insights from fluorescence spectroscopy, electrochemical measurement and molecular docking. Spectrochim Acta A Mol Biomol Spectrosc. 2015;149:536–543. https://doi.org/10.1016/j.saa.2015.04.087.
37. Kahveci Z, Martínez-Tomé MJ, Mallavia R, Mateo CR. Use of the conjugated polyelectrolyte poly {[9, 9-bis (6′-n, n, n-trimethylammonium) hexyl] fluorene-phenylene} bromide (htma-pfp) as a fluorescent membrane marker. Biomacromolecules. 2013;14(6):1990–1998. https://doi.org/10.1021/bm400348n.
38. Simon J, Udayan S, Bindiya E, Bhat SG, Nampoori V, Kailasnath M. Optical characterization and tunable antibacterial properties of gold nanoparticles with common proteins. Anal Biochem. 2021;612:113975. https://doi.org/10.1016/j.ab.2020.113975.
39. Gebauer JS, Malissek M, Simon S, Knauer SK, Maskos M, Stauber RH, Peukert W, Treuel L. Impact of the nanoparticle–protein corona on colloidal stability and protein structure. Langmuir. 2012;28(25):9673–9679. https://doi.org/10.1021/la301104a.
40. Yin Z, Wu Y, Chen Y, Qie X, Zeng M, Wang Z, Qin F, Chen J, He Z. Analysis of the interaction between cyanidin-3-o-glucoside and casein hydrolysates and its effect on the antioxidant ability of the complexes. Food Chem. 2021;340:127915. https://doi.org/10.1016/j.foodchem.2020.127915.
41. Yin M-M, Chen W-Q, Lu Y-Q, Han J-Y, Liu Y, Jiang F-L. A model beyond protein corona: thermodynamics and binding stoichiometries of the interactions between ultrasmall gold nanoclusters and proteins. Nanoscale. 2020;12(7):4573–4585. https://doi.org/10.1039/C9NR09170J.
42. Ross PD, Subramanian S. Thermodynamics of protein association reactions: forces contributing to stability. Biochemistry. 1981;20(11):3096–3102. https://doi.org/10.1021/bi00514a017.